Microscopic Marangoni Flows Cannot Be Predicted on the Basis of Pressure Gradients

Yawei Liu,[1,2] Raman Ganti,[3] Hugh G. A. Burton,[3] Xianren Zhang,[2] Wenchuan Wang,[1] and Daan Frenkel[3,*]

[1]*Beijing Advanced Innovation Center for Soft Matter Science and Engineering,
Beijing University of Chemical Technology, Beijing 100029, People's Republic of China*
[2]*State Key Laboratory of Organic-Inorganic Composites, Beijing University of Chemical Technology,
Beijing 100029, People's Republic of China*
[3]*Department of Chemistry, University of Cambridge, Lensfield Road, Cambridge CB2 1EW, United Kingdom*

A concentration gradient along a fluid-fluid interface can cause flow. On a microscopic level, this so-called Marangoni effect can be viewed as being caused by a gradient in the pressures acting on the fluid elements or as the chemical-potential gradients acting on the excess densities of different species at the interface. If the interface thickness can be ignored, all approaches should result in the same flow profile away from the interface. However, on a more microscopic scale, the different expressions result in different flow profiles, only one of which can be correct. Here we compare the results of direct nonequilibrium molecular dynamics simulations with the flows that are generated by pressure and chemical-potential gradients. We find that the approach based on the chemical-potential gradients agrees with the direct simulations, whereas the calculations based on the pressure gradients do not.

Fluid flows can be generated by variations of temperature or solute concentration parallel to a fluid-fluid interface. This phenomenon is known as the Marangoni effect (see, e.g., Refs. [1,2]). The "continuum" explanation for this effect is that the gradients in temperature or concentration result in gradients in the surface tension, which then induce shear flow [3–9]. For some applications, it would be interesting to have a higher-resolution description of Marangoni flows. The reason is that the local shear in Marangoni flows can be quite large and could become important for nanofluidics [10–13]. Moreover, the precise Marangoni flow profile might affect the orientation and even conformation of molecules such as proteins near an interface. At present, such microscopic insights in Marangoni flows are lacking.

In this Letter, we study the flow induced in a flat liquid-liquid interface by the concentration gradient of a neutral solute (i.e., the "solutal" Marangoni effect). We first review the various (pressure- or chemical-potential-based) expressions for the force acting on molecules near the interface. We then perform molecular dynamics (MD) simulations to compare the flows generated by these forces with the results of direct nonequilibrium simulations with explicitly imposed concentration gradients.

Let us first consider two immiscible liquids at temperature T that meet at a flat liquid-liquid interface at $z(x, y) = 0$. When a concentration gradient is applied along x, flow occurs due to a surface-tension gradient. The surface tension γ can be related to the integral of the difference between the longitudinal and transverse pressures near the interface,

$$\gamma = \int_{-\infty}^{+\infty} [p^{zz}(z) - p^{xx}(z)]dz, \tag{1}$$

where $p^{zz}(z)$ and $p^{xx}(z)$ are the normal and transverse components of the pressure tensor at z, respectively [14–16]. Below, we will discuss different definitions of the pressure tensor. However, as was pointed out by Schofield and Henderson [17], the integral in Eq. (1) does not depend on the choice of the expression for the pressure tensor. Nevertheless, the microscopic flow near an interface is expected to depend on the local gradients of the pressure rather than the gradients of the integral of the pressure tensor. This is important because, close to the interface, the viscosity of the liquid need not be constant, hence, making a difference where the forces act.

The most intuitive method to obtain the Marangoni force acting on fluid molecules near the interface is to calculate the force per unit volume on a small volume element from the pressure gradient $[\partial p^{xx}(z)/\partial x]$ and then obtain the force per particle by dividing the force per volume by the local number density. We now make the assumption that $p^{xx}(z)$ depends on x only through its dependence on the spatial variation in the bulk concentration ρ_C (or, equivalently, the chemical potential) of the species subject to a concentration gradient:

$$f^V(z) = -\frac{\partial p^{xx}(z)}{\partial \rho_C} \frac{\partial \rho_C}{\partial x}. \tag{2}$$

We note that the condition for mechanical equilibrium in the bulk implies, via the Gibbs-Duhem relation, that a concentration gradient in a solute also causes a gradient in the concentration of the solvent. However, these other gradients are not independent, and, hence, we will treat the solute concentration gradient as the independent variable.

The general expression for the local pressure tensor at position **r** is given by

$$p^{ab}(\mathbf{r}) = \rho(\mathbf{r})k_B T \delta^{ab} + \frac{1}{V}\left\langle \sum_i \sum_{j>i} r_{ij}^a f_{ij}^b \xi^{ab}(\mathbf{r}, \mathbf{r}_i, \mathbf{r}_j) \right\rangle$$

(3)

under the condition of $\int d\mathbf{r}\, \xi^{ab}(\mathbf{r}, \mathbf{r}_i, \mathbf{r}_j) = 1$ [17–19]. Here, a and b denote the Cartesian components of the pressure tensor, $\rho(\mathbf{r})$ is the local density, δ^{ab} denotes the Kronecker delta, r_{ij} and f_{ij} represent the distance and force between particles i and j, and $\xi^{ab}(\mathbf{r}, \mathbf{r}_i, \mathbf{r}_j)$ is the fraction of the intermolecular virial from a given pair of molecules at $\mathbf{r}_i$ and $\mathbf{r}_j$ to be assigned to position $\mathbf{r}$. As was argued in Ref. [17], there is no unambiguous way to assign the intermolecular virial in the system. All definitions of the pressure tensor that differ only by a function that is divergence-free are acceptable. There are, in fact, several widely used definitions for the local pressure tensor [15,20]. For example, for a given pair of molecules, the virial definition specifies that half of the contribution to the stress resides in each elemental volume containing the molecule [21], while the Irving-Kirkwood definition specifies that the contribution is evenly distributed along a line connecting the two molecules [18]. These two definitions lead to the same value of the surface tension but to very different results for the pressure-tensor distribution in the interface [22,23].

Gibbs was the first to give a consistent thermodynamic description of the surface tension [24]. In particular, Gibbs related the variation of the surface tension with the chemical potential of species i to the excess of that species at the interface. For an n-component system: $d\gamma = -\sum_{i=1}^{n} \Gamma_i d\mu_i$, with Γ_i the surface excess and $d\mu_i$ the chemical-potential variation due to the concentration gradient. We assume that $\partial\mu_i/\partial x$ is independent of z (fast equilibration normal to the interface). Because $\Gamma_i \equiv \int_{-\infty}^{\infty} (\rho_i(z,x) - \rho_i^{\text{bulk}}(x))dz$, the surface-tension gradient along x is

$$\frac{\partial\gamma}{\partial x} = \int_{-\infty}^{\infty} \sum_{i=1}^{n} (\rho_i(z,x) - \rho_i^{\text{bulk}}(x))\left(-\frac{\partial\mu_i}{\partial x}\right)dz.$$

(4)

This suggests that the local force acting on a volume element at **r** is given by $-\sum_{i=1}^{n} \Gamma_i(\mathbf{r})(-\partial\mu_i/\partial x)$. Such a relation also follows from the Gibbs-Duhem equation $V dp = \sum_{i=1}^{n} N_i d\mu_i$ with N_i the number of particles of component i in volume V and p the pressure. Let us denote the number density of component i in the mixture by ρ_i. Then $dp = \sum_{i=1}^{n} \rho_i d\mu_i$. A concentration gradient of component i along x will lead to a chemical-potential gradient $\partial\mu_i/\partial x$. As the pressure remains constant in the bulk, we must have $0 = \sum_{i=1}^{n} \rho_i^{\text{bulk}}(x)(\partial\mu_i/\partial x)$. At a position z near the interface, a pressure gradient remains giving a force per unit volume

$$f^V(z) = \left(-\frac{\partial p^{xx}(z,x)}{\partial x}\right)$$

$$= \sum_{i=1}^{n} (\rho_i(z,x) - \rho_i^{\text{bulk}}(x))\left(-\frac{\partial\mu_i}{\partial x}\right).$$

(5)

We can interpret $(-\partial\mu_i/\partial x)$ as the force per atom acting on the particles of component i. This expression is convenient because the imposed chemical-potential gradients are constant throughout the system. In the bulk, the composition is such that the forces balance (because the bulk pressure equilibrates rapidly). Upon approaching the interface, the concentration of different components may change, leading to nonzero net forces. In other words, particles of a given species experience the same force regardless of their distance from the interface. The force acting on species i is then

$$f_i = \left(-\frac{\partial\mu_i^{\text{bulk}}}{\partial x}\right) = \left(-\frac{\partial\mu_i^{\text{bulk}}}{\partial\rho_i}\right)_P \nabla\rho_i.$$

(6)

We now have two alternative expressions [Eqs. (2) and (5)] for the surface force arising in the solutal Marangoni effect. Both satisfy that the integrated surface force is equal to the surface-tension gradient, but otherwise they are not obviously identical.

To test which, if any, of these microscopic expressions is correct, we performed MD simulations on a simple model system. We consider a fluid mixture composed of one solute (C) and two immiscible solvents (A and B, respectively), with two liquid-liquid interfaces, as shown in Fig. 1. All particles are assumed to have the same mass m and molecular radius σ. They interact through Lennard-Jones potentials $U_{\alpha\beta}(r) = 4\epsilon_{\alpha\beta}[(\sigma/r)^{12} - (\sigma/r)^6]$ ($\alpha, \beta \in \{A, B, C\}$) with interaction energy $\epsilon_{\alpha\beta}$. All interactions are truncated and shifted at 4σ. For simplicity, we focus on ideal solutions composed of identical solvent and solute particles and take $\epsilon_{AA} = \epsilon_{BB} = \epsilon_{CC} = \epsilon_{AC} = \epsilon_{BC} \equiv 1.0\epsilon$ (which defines
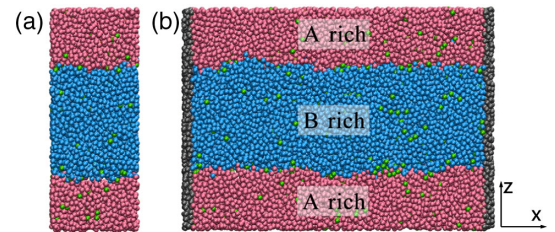

FIG. 1. (a) Simulation box used in the equilibrium MD simulations to compute the forces using Eqs. (6) and (7), and in the nonequilibrium MD simulations with explicit forces to measure flow profiles generated by these forces. (b) Simulation box used in the direct nonequilibrium MD simulations with explicitly imposed concentration gradients. The red and blue particles represent the two solvents (A and B), the green particles represent the solute (C), and the black particles represent the solid walls.

our unit of energy). However, A and B tend to demix because they have a weaker attraction: $\epsilon_{AB} = 0.3\epsilon$. Throughout this Letter, we use reduced units with σ, ϵ, and m denoting the units of length, energy, and mass, respectively.

All simulations were carried out using LAMMPS [25] in an isothermal, isobaric ($Np^{zz}T$) ensemble. Periodic boundary conditions were imposed in all directions. The temperature and normal pressure during the simulations were maintained at $T = 0.846$ and $p_{ex} = 0.012$. The relaxation parameter for the Nosé-Hoover thermostat is set to 0.1 and that for the pressure barostat is 1. The velocity-Verlet algorithm with a time step of 0.001 is used for the integration of equations of motion. All simulations were run for $(2 \times 10^8) - (4 \times 10^8)$ steps to obtain good statistics.

The computation of $\partial p^{xx}(z)/\partial\rho_C$ requires several equilibrium simulations at a constant bulk concentration. These can be carried out in a relatively small simulation box shown in Fig. 1(a). The box dimensions were $L_x = 16.44$ and $L_y = 9.86$, $\langle L_z \rangle = 42.4$ (L_z fluctuates and depends very weakly on the solute concentration). The system contained 5040 particles, approximately equally distributed between the A phase and the B phase. To compute the composition dependence of $p^{xx}(z)$, we performed simulations where we varied the concentration of the solute C, while keeping the total number of particles fixed.

From the numerical estimate of $\partial p^{xx}(z)/\partial\rho_C$, we computed the corresponding force at $\rho_C = 0.02$ and $\Delta\rho_C = 0.01$ using

$$f^V(z) = -\frac{\partial p^{xx}(z)}{\partial\rho_C}\frac{\partial\rho_C}{\partial x}$$
$$\approx -\frac{p^{xx}_{\rho_C+\Delta\rho_C}(z) - p^{xx}_{\rho_C-\Delta\rho_C}(z)}{2\Delta\rho_C}\nabla\rho_C. \quad (7)$$

We verified that our estimate for the pressure gradient did not depend on our choice of $\Delta\rho_C$. Subsequently, we converted the force per unit volume to a force per particle by dividing by the total number density at height z, $\rho(z)$. These per-particle forces were then applied in a nonequilibrium simulation with solute density ρ_C in the box, as shown in Fig. 1(a), to measure the corresponding flow profile at $\nabla\rho_C$.

Starting from Eq. (6), we can compute the forces that would result from the gradient of the chemical potentials. These per-atom forces were applied to the solute and the solvent particles. During all these simulations with explicit forces [Fig. 1(a)], a constant force is applied to all fluid particles to balance the surface force to ensure that there is no center-of-mass flow. To measure the local velocity, the simulation box was divided into a series of slabs of thickness $dz = 0.05$ parallel to the interface. The local velocity is computed as the time-averaged center-of-mass velocity of all fluid particles in each slab.

To compare, we performed *direct* nonequilibrium simulations where a concentration gradient was explicitly imposed. Here, "direct" is used to refer to such simulations that differ from above nonequilibrium simulations with explicit forces. Figure 1(b) shows the simulation box in which the fluid mixture has a constant bulk concentration gradient along x. The box size $L_x = 59.19$ and $L_y = 9.86$, and $\langle L_z \rangle = 42.4$. The system contained 18144 particles, approximately equally distributed between the A phase and the B phase. Direct nonequilibrium simulations were carried out to measure the flow profile at a given value of $\nabla\rho_C$. In this case, we employed a box that was terminated on both ends by hard walls perpendicular to the x direction. These walls were composed of frozen fluid particles that interact with the fluid via Lennard-Jones potentials where $\epsilon_{WA} = \epsilon_{WB} = \epsilon_{WC} = 1.0\epsilon$. Next to each wall, we defined a "source" region with a width of 8. During the simulations, every 500 steps, the types of the fluid particles in the bulk of these source regions are reset to maintain constant bulk concentrations on the two sides and a steady gradient along x. In the simulation, flow in the interface set in motion by the surface force is accompanied by a bulk backflow caused by the presence of the walls. Moreover, the fluid states are still close to equilibrium, and the equilibration of each species along z is very fast (see the Supplemental Material S1 [26]).

In order to calculate the surface force at $\rho_C \sim 0.02$ via Eq. (2), we computed the pressure-tensor profile at $\rho_C \sim 0.01$ and $\rho_C \sim 0.03$. Figure 2 shows the pressure profiles along z near a liquid-liquid interface at $\rho_C \sim 0.01$ using the Irving-Kirkwood and virial definitions. In the bulk where the fluid is homogeneous, both definitions lead to the same value since $p^{zz} = p^{xx} = p_{ex} = 0.012$. Upon approaching the interface, p^{zz} from the Irving-Kirkwood definition is (necessarily) the same as the bulk pressure, reflecting mechanical equilibrium along z [Fig. 2(a)]. As is well known, the virial expression for p^{zz} is not constant [Fig. 2(b)]. We verified that the two expressions for the pressure tensor did yield the same value of surface tension. We find [from Eq. (1)] that the surface tension is 1.14 at $\rho_C \sim 0.01$ and 1.05 at $\rho_C \sim 0.03$.

The chemical potential for component i is given by $\mu_i = \mu_i^0 + k_B T \ln \rho_i^{bulk} + \mu_i^{exc}$, with k_B the Boltzmann constant, μ_i^0 denotes a (constant) reference value, and μ_i^{exc} denotes the excess chemical potential due to intermolecular interactions. Because the bulk solutions are ideal, μ_i^{exc} does not depend on the concentration of C. Thus, at $\rho_C \sim 0.02$, with $\rho_A^{bulk} = \rho_B^{bulk} = 0.742$ and $\rho_C^{bulk} = 0.019$ [Fig. S1(b) [26]], if $\nabla\rho_C = 1.0$, we obtain $f_A = f_B = 1.14$ and $f_C = -44.53$ from Eq. (5) (i.e., we do, indeed, have force balance in the bulk).

We are now in a position to compare the force profiles that follow from the pressure-tensor gradients with those that follow from the chemical-potential gradient. Figure 2(c) shows the profiles of the volume force at $\rho_C \sim 0.02$ with $\nabla\rho_C = 1.0$. As can be seen from the figure, the two expressions for the surface force [Eqs. (2) and (5)]
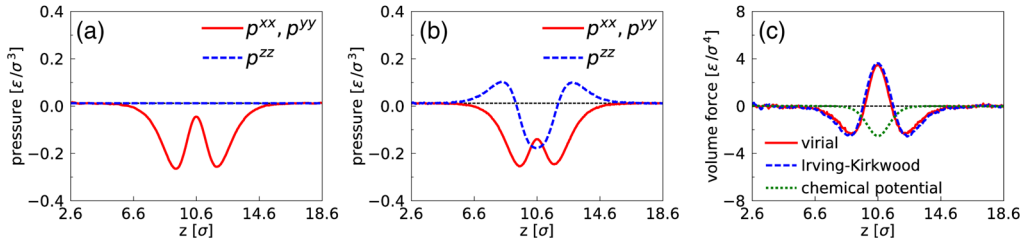
FIG. 2.   (a), (b) The pressure profiles along z near one interface at $z = 10.6$ calculated by the Irving-Kirkwood definition (a) and virial definition (b) at $\rho_C \sim 0.01$. The black dashed line shows the external pressure of $p_{ex} = 0.012$. (c) The volume force profiles per unit concentration gradient along z near one interface at $z = 10.6$ calculated by different methods at $\rho_C \sim 0.02$. The horizontal dashed line corresponds to the force of zero.

produce significantly different results at the interface. Not surprisingly, the forces calculated from the chemical potentials [Eq. (5)] are concentrated where there is an excess of solute [Fig. S1(b) [26]]. However, the forces calculated by using the local pressure tensors computed via the Irving-Kirkwood and virial definitions [Eq. (2)] extend over larger distances and vary in sign. The Irving-Kirkwood and virial definitions lead to force profiles that are very similar. We verified that the integrated Marangoni force is effectively the same for all methods used: -4.7 ± 0.1 for the chemical potential, -4.8 ± 0.1 for the virial, and -4.8 ± 0.1 for the Irving-Kirkwood, respectively. Moreover, these values agree with the surface-tension gradient calculated from the values of surface tension at different concentrations, which is -4.8 ± 0.1 at $\rho_C \sim 0.02$ with $\nabla\rho_C = 1.0$ [calculated via $(\partial\gamma/\partial\rho_C)\nabla\rho_C$].

The fact that pressure-tensor and chemical-potential routes lead to different force profiles implies that they would result in different flow profiles. At most, one can be correct. To test this, we applied the force profiles that we computed to the fluid mixture at $\rho_C \sim 0.02$ and measured the flow profile as a function of z for fixed $\nabla\rho_C$. The Irving-Kirkwood and virial definitions lead to very similar results for the surface force, and, hence, we show only the virial flow profile. Figure 3(a) shows the predicted velocity profiles at $\nabla\rho_C = 0.001$. We see that although the velocity profiles are very similar in the bulk, they are significantly different near the interface. For the sake of comparison, the velocity profile obtained in a direct nonequilibrium MD simulation with an imposed concentration gradient of $\nabla\rho_C = 0.001$ was determined in a region with $-10 < x < 10$ ($x = 0$ at the center of the box). The result is shown in Fig. 3(b). We see that the velocity profile that follows from the direct simulation differs markedly from the one obtained from the pressure-tensor gradients. However, it agrees quite well with the predictions based on the chemical-potential gradient calculations. The same results were found at $\nabla\rho_C = 0.0005$ (Fig. S2 [26]).

This finding is interesting because it indicates that the use of local pressure-tensor gradients leads to incorrect prediction of the Marangoni flow profile near the interface, even though the velocity in the bulk is still reliable. The latter finding is consistent with our previous work [27],

which showed that bulk thermo-osmotic flow computed via local pressure gradients agrees well with the flow predicted by its reciprocal mechanocaloric coefficient. Our results suggest that the chemical-potential route should be the preferred route to compute microscopic Marangoni flows.

On the other hand, pressure tensors are extremely useful in the description of bulk hydrodynamic phenomena, and the present microscopic expressions for the stress are widely used in molecular simulations, both for the study of bulk properties (e.g., elastic stresses [28,29]) and for the computation of the surface tension of fluids [22,23]. However, the failure of the pressure tensor revealed here suggests that they should clearly be handled with care on
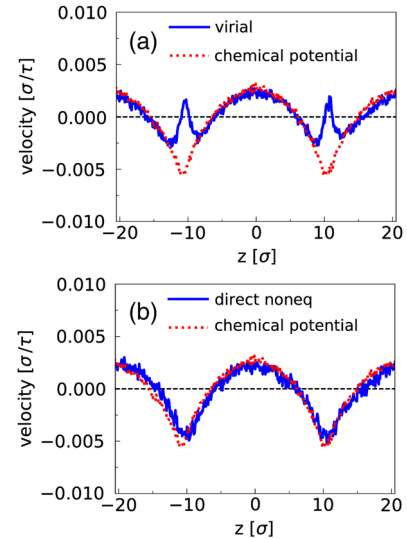

FIG. 3.   The velocity profiles along z from different approaches at $\nabla\rho_C = 0.0010$: (a) pressure-tensor and chemical-potential routes, (b) direct-nonequilibrium and chemical-potential routes. The horizontal dashed line corresponds to the velocity of zero. Here, "virial" represents the velocity profile from the nonequilibrium simulation with explicitly imposed forces, and the forces are calculated from the virial pressure gradient [Eq. (7)]. "Chemical potential" represents the velocity profile from the nonequilibrium simulation with explicit forces, but the forces are calculated from the chemical-potential gradient [Eq. (6)], while "direct noneq" represents the velocity profile from the direct nonequilibrium simulation with explicitly imposed concentration gradient.

the microscopic scale. In their original hydrodynamic formulation of the stress tensor [18], Irving and Kirkwood note that a boundary or interface can cause the stress to depend on gradients of the pairwise atomic density, which can be neglected in the standard Irving-Kirkwood expression for fluids in the absence of gradients. The present work provides evidence that the problem hinted at by Irving and Kirkwood indeed becomes important in a gradient near an interface, as the potential part of the stress tensor then depends not only on the distance of two points between which a force acts but also on the absolute coordinates of these points. Yet, the fact that both the Irving-Kirkwood and virial expressions for the microscopic stress yield the same incorrect answer, strongly suggests that minor tweaks to either will not be enough to fix the problem [17]. We hope that our work will inspire others to think about other solutions and possibly arrive at a formulation that allows one to calculate the Marangoni flow from the knowledge of the gradient of another, as yet unknown, microscopic function.

*Corresponding author.
df246@cam.ac.uk

[1] M. Loewenthal, Philos. Mag. J. Sci. **12**, 462 (1931).
[2] A. V. Hershey, Phys. Rev. **56**, 204 (1939).
[3] N. O. Young, J. S. Goldstein, and M. J. Block, J. Fluid Mech. **6**, 350 (1959).
[4] C. V. Sternling and L. E. Scriven, AIChE J. **5**, 514 (1959).
[5] V. G. Levich, *Physicochemical Hydrodynamics* (Prentice-Hall, Englewood Cliffs, NJ, 1962).
[6] V. G. Levich and V. S. Krylov, Annu. Rev. Fluid Mech. **1**, 293 (1969).
[7] E. Ruckenstein, J. Colloid Interface Sci. **83**, 77 (1981).
[8] J. Anderson, Annu. Rev. Fluid Mech. **21**, 61 (1989).
[9] X. Fanton and A. M. Cazabat, Langmuir **14**, 2554 (1998).
[10] H. Stone, A. Stroock, and A. Ajdari, Annu. Rev. Fluid Mech. **36**, 381 (2004).
[11] T. M. Squires and S. R. Quake, Rev. Mod. Phys. **77**, 977 (2005).
[12] L. Bocquet and E. Charlaix, Chem. Soc. Rev. **39**, 1073 (2010).
[13] L. Bocquet and P. Tabeling, Lab Chip **14**, 3143 (2014).
[14] R. C. Tolman, J. Chem. Phys. **16**, 758 (1948).
[15] J. Kirkwood and F. Buff, J. Chem. Phys. **17**, 338 (1949).
[16] A. Marchand, J. H. Weijs, J. H. Snoeijer, and B. Andreotti, Am. J. Phys. **79**, 999 (2011).
[17] P. Schofield and J. R. Henderson, Proc. R. Soc. A **379**, 231 (1982).
[18] J. H. Irving and J. G. Kirkwood, J. Chem. Phys. **18**, 817 (1950).
[19] G. J. Gloor, G. Jackson, F. J. Blas, and E. de Miguel, J. Chem. Phys. **123**, 134703 (2005).
[20] A. Harasima, J. Phys. Soc. Jpn. **8**, 343 (1953).
[21] M. J. P. Nijmeijer, A. F. Bakker, C. Bruin, and J. H. Sikkenk, J. Chem. Phys. **89**, 3789 (1988).
[22] J. Walton, D. J. Tildesley, J. S. Rowlinson, and J. R. Henderson, Mol. Phys. **48**, 1357 (1983).
[23] J. Weng, S. Park, J. R. Lukes, and C. Tien, J. Chem. Phys. **113**, 5917 (2000).
[24] J. W. Gibbs, *The Collected Works of J. Willard Gibbs* (Yale University Press, New Haven, CT, 1957).
[25] S. Plimpton, J. Comput. Phys. **117**, 1 (1995).
[26] See the Supplemental Material at http://link.aps.org/supplemental/10.1103/PhysRevLett.119.224502 for fluid states in direct nonequilibrium simulations and flow profiles at another concentration gradient.
[27] R. Ganti, Y. Liu, and D. Frenkel, Phys. Rev. Lett. **119**, 038002 (2017).
[28] A. K. Subramaniyan and C. Sun, Int. J. Solids Struct. **45**, 4340 (2008).
[29] M. Tsamados, A. Tanguy, C. Goldenberg, and J.-L. Barrat, Phys. Rev. E **80**, 026112 (2009).